Heliyon 10 (2024) e33084

Contents lists available at ScienceDirect

Heliyon

journal homepage: www.cell.com/heliyon

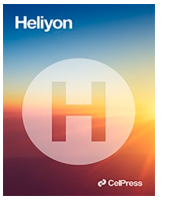

Research article

LncR-GAS5 decrease in adenine phosphoribosyltransferase expresssion via binding TAF1 to increase kidney damage created by CIH

Wei Liu [a,b], Wukaiyang Liang [a,b], CunTai Zhang [a,b], Huiguo Liu [c], Hai Li [a,b], Lun Zhou [a,b,**], Ling Zhou [c,*]

[a] *Department of Geriatrics, Tongji Hospital, Tongji Medical College, Huazhong University of Science and Technology, 1095 Jiefang Avenue, Wuhan, 430030, China*

[b] *Key Laboratory of Vascular Aging, Ministry of Education, Tongji Hospital, Tongji Medical College, Huazhong University of Science and Technology, 1095 Jiefang Avenue, Wuhan, 430030, China*

[c] *Department of Respiratory and Critical Care Medicine, Key Laboratory of Pulmonary Diseases of Health Ministry, Tongji Hospital, Tongji Medical College, Huazhong University of Science and Technology, Wuhan, 430030, China*

ARTICLE INFO

Keywords:
lncRNA GAS5
TAF1
APRT
CIH
Renal injury

ABSTRACT

Objective: Chronic kidney disease (CKD) related to obstructive sleep apnea-hypopnea syndrome (OSAHS) mainly results from chronic intermittent hypoxia (CIH)-induced renal injury. This study aimed to explore the interaction between the long noncoding RNA (lncRNA) growth arrest-specific transcript 5 (GAS5) and recombinant adenine phosphoribosyltransferase (APRT) in CIH-induced renal injury.

Methods: A rat intermittent hypoxia model was constructed, total RNA was extracted from kidney tissue, and transcriptome sequencing was performed using high-throughput sequencing technology. CIH rat models were established and injected with sh-GAS5 or OE-APRT plasmid, the serum levels of blood urea nitrogen (BUN) and creatinine amidohydrolase were measured, and the expression of oxidative stress-related factors was detected. Hematoxylin and eosin (H&E) and Masson's trichrome staining were used for morphological observations, and cell apoptosis was determined by TUNEL staining. Interactions between GAS5, TATA-box binding protein-associated factor 1 (TAF1), and APRT were predicted and verified. After transfection of HK-2 cells, the expression of GAS5, TAF1, APRT, Bax, Bcl-2, apoptosis-related factors, fibrosis-related factors (collagen I and IV), and autophagy-related proteins (LC3-II, LC3-I, p62, and Beclin-1) was measured by RT-qPCR and western blotting.

Results: Sequencing results revealed that TAF1 was significantly increased and APRT was significantly decreased in the CIH group. RNA was significantly involved in the biological process of kidney injury mediated by CIH. CIH rats injected with GAS5 suppression or APRT overexpression plasmids showed decreased GAS5 and elevated APRT expression, along with suppressed serum levels of BUN and creatinine amidohydrolase. Meanwhile, GAS5 suppression or APRT overexpression attenuated apoptosis and fibrosis, suppressed oxidative stress, and

* Corresponding author. Department of Respiratory and Critical Care Medicine, Key Laboratory of Pulmonary Diseases of Health Ministry, Tongji Hospital, Tongji Medical College, Huazhong University of Science and Technology, Wuhan, 430030, China

** Corresponding author. Department of Geriatrics, Tongji Hospital, Tongji Medical College, Huazhong University of Science and Technology, 1095 Jiefang Avenue, Wuhan, 430030, China.

E-mail addresses: zhoulun79@sina.com (L. Zhou), 471699217@tjh.tjmu.edu.cn (L. Zhou).

https://doi.org/10.1016/j.heliyon.2024.e33084
Received 16 January 2024; Received in revised form 13 June 2024; Accepted 13 June 2024
Available online 14 June 2024

promoted autophagy in CIH-induced renal tubular epithelial cells. The RNA pull-down assay and RIP verified the binding and interaction of GAS5 and TAF1. Chip immunoprecipitation (ChIP) identified TAF1 regulation of the APRT promoter. GAS5 and TAF1 negatively regulated APRT expression.

Conclusion: The lncRNA GAS5 can bind TAF1 to suppress APRT transcription, thereby enhancing CIH-induced renal injury in rats.

1. Introduction

Obstructive sleep apnea-hypopnea syndrome (OSAHS) is a sleep-related breathing disorder characterized by snoring and the repetitive collapse of the upper airways, which disrupts normal ventilation [1,2]. OSAHS is associated with multiple comorbidities, including cardiovascular events and chronic kidney disease (CKD). OSAHS damages renal tubular function; promotes renal inflammation, endothelial dysfunction, and renal fibrosis through chronic hypoxemia; activates the sympathetic nervous system or renin-angiotensin-aldosterone system (RAAS); induces the production of reactive oxygen species; and ultimately leads to renal function damage. The incidence of OSAHS is high in patients with CKD, and OSAHS promotes CKD progression. More than half of patients with CKD have OSAHS, which in turn results in unfavorable progression and increased mortality [3,4]. Therefore, CKD and OSAHS have a bidirectional relationship [5]. Chronic intermittent hypoxia (CIH) plays a key role in activating the sympathetic nervous system or RAAS in renal tissue and eventually progresses to CKD [6]. Therefore, CIH-induced renal injury related to OSAHS is a major contributor to CKD progression, and elucidation of its possible pathology is of great importance for the treatment of OSAHS-related CKD.

The lncRNA growth arrest-specific 5 (GAS5) was initially identified in growth-arrested cells [7] and is crucial for numerous signaling pathways [8]. The tumor-suppressive effect of GAS5 has also been observed in various tumor types, including gastric [9] and colorectal [10] cancer. However, the role of GAS5 in clear cell renal cell carcinoma remains controversial. In a previous study, GAS5 suppression enhanced the tumorigenicity of clear cell renal cell carcinoma [11,12], while another study identified GAS5 overexpression in clear cell renal cell carcinoma tissues [13]. Furthermore, the role of GAS5 in renal fibrosis remains controversial [14]. However, the mechanism of action of GAS5 in intermittent hypoxia remains unclear. Therefore, in the present study, we aimed to determine the role and effects of GAS5 in CIH-induced renal injury.

Deficiency of adenine phosphoribosyltransferase (APRT) is a disorder associated with purine metabolism that mainly affects kidney function [15]. APRT deficiency contributes to the development of kidney stones and CKD in young children [16]. However, no study has explored the role of APRT in OSAHS. (TATA-box binding protein-associated factor 1) TAF1 is a subcomplex of transcription factor IID (TFIID) that is involved in the recognition of DNA initiators and promoter elements [17]. The GAS5-TAF1 feedback loop inhibits the osteogenic differentiation of human bone marrow mesenchymal stem cells [18]. The LncMAP database has predicted a possible interaction between GAS5, TAF1, and APRT in papillary renal cell carcinoma; therefore, we speculated that GAS5 may also regulate TAF1 and APRT in CIH-induced renal injury. This study aimed to verify the possible role of the GAS5/TAF1/APRT axis in CIH-induced renal injury in both cell lines and rat models.

2. Materials and methods

2.1. CIH model establishment

The day and night habits, nocturnal movement, and sleep times of Sprague-Dawley (SD) rats were consistent with people's working hours; therefore, SD rats were suitable for the study of OSA. SD rats (180–220 g) were purchased from GemPharmatech (Jiangsu, China; Laboratory Animal Production Certificate No: SCXK [Jing] 2021-0106). Rats were housed with a light-dark (12 h:12 h) cycle at $22 \pm 3\ ^{\circ}C$, 60 ± 5 % humidity, and free access to food and water. The experimental design was approved by the ethics committee of the Animal Care and Use Committee of Tongji Hospital.

The oxygen sensor was placed under the CIH cabin to measure oxygen. From 8 a.m. to 4 p.m., the rats were exposed to 5 % O_2 for 2 min, 4 min per cycle, for 8 h. Establishing the CIH model took eight weeks [19]. CIH rats in the CIH + sh-GAS5 or CIH + OE-APRT groups received caudal vein injections of 2 mg/kg sh-GAS5 (GeneChem, Shanghai, China) or OE-APRT (GeneChem, Shanghai, China) plasmids, respectively. Rats in both groups were euthanized with ketamine and xylazine on the fifteenth day after the last anoxia cycle. The renal tissues were collected for morphological analysis.

2.2. Serum biochemical indicators

Venous blood from the abdomen was collected and centrifuged at 3000 rpm for 10 min, and the serum on the surface was collected. Serum levels of urea nitrogen (BUN) and creatinine were measured using BUN (EIABUN, Invitrogen, New York, USA) and creatinine (C011-2-1, Nanjing Jiancheng Bioengineering Institute, Jiangsu, China) kits, respectively, to assess renal function.

2.3. Determination of oxidative stress parameters

Renal tissues were homogenized using a homogenizer. Superoxide dismutase (SOD; S0101S, Beyotime, Shanghai, China), malondialdehyde (MDA; S0131S, Beyotime), glutathione peroxidase (GSH-px; S0058, Beyotime), GSH, and glutathione disulfide (GSSG; S0053, Beyotime) kits were used to detect the expression levels of the oxidative parameters in the homogenate.

2.4. Hematoxylin & eosin (H&E) staining

The bilateral kidneys were perfused with normal saline through the abdominal aorta until no blood flowed out. The kidneys were fixed in 4 % paraformaldehyde, embedded in paraffin, and sectioned. The sections were deparaffinized and washed with decreasing ethanol gradients (100 %, 95 %, 80 %, and 75 %). Sections were stained with hematoxylin (2 g/L) for 5 min, washed with distilled water, and immersed in hydrochloric acid/ethanol (1 mL hydrochloric acid with 99 mL 70 % ethanol) for 30 s. Sections were then immersed in distilled water for 15 min and stained with a 1 % eosin solution for 2 min before washing with distilled water. The slices were then hydrated with absolute ethanol and sealed with neutral resin. Images were captured using an Inverted Olympus microscope. Renal injury was scored according to the modified 0–5 Jablonski scale: 0, normal cells; 1, individual cell degeneration and necrosis; 2, cell degeneration and necrosis of one kidney tubule; 3, cell degeneration and necrosis adjacent to the proximal convoluted tubule with surviving cells surrounding the tubule; 4, necrosis limited to one-third of the distal convoluted tubule and one necrosis band extended to the inner cortex; and 5, cell necrosis in all segments of the proximal convoluted tubule [20].

2.5. Masson's staining

Deparaffinized slices were stained with Weigert's iron hematoxylin solution for 5 min and differentiated with acetic alcohol before washing under running water. The slices were stained with Ponceau solution for 5 min, followed by treatment with phosphomolybdic acid for 3 min, and toluidine blue O for 5 min. Before dehydration and sealing, the slices were immersed in 1 % glacial acetic acid for 1 min. The sections were observed under a microscope.

2.6. TdT-mediated dUTP nick end labeling(TUNEL) staining

The kidney slices were incubated with 50 μL of 0.1 % Triton X-100 at room temperature for 8 min and then washed in PBS, before antigen retrieval with citric acid-sodium citrate solution. Next, slices were incubated with 50 μL TUNEL solution at 37 °C for 60 min and then incubated with goat serum for 30 min. Then, CD31 primary antibody (1:200, ab9498, Abcam, Cambridge, UK) was incubated with the slices overnight at 4 °C, followed by incubation with the secondary antibody (1:200, ab150088, Abcam) at room temperature for 60 min. The excess antibody was washed away, and the slices were stained with DAPI (20 mg/mL, D9542, Sigma, Germany), after which the antifade mounting medium was added for cell counting under a microscope.

2.7. Cell culture and transfection

HK-2 cells retain the well-differentiated phenotype and functional properties of proximal renal tubular epithelial cells and were used to establish a hypoxia-reoxygenation model that mimics the process of renal ischemia-reperfusion injury. Human proximal tubular cells (HK-2), purchased from Shanghai Cell Bank of Chinese Academy of Sciences, were cultured in RPMI1640 (72400120, Gibco, New York, USA) with 10 % FBS (16140071, Gibco) at 37 °C in an incubator supplemented with 5 % CO_2.

Plasmids with GAS5 overexpression (OE-GAS5), GAS5 inhibition (sh-GAS5), TAF1 overexpression (OE-TAF1), TAF1 inhibition (sh-TAF1), APRT overexpression (OE-APRT), and APRT inhibition (sh-APRT) and negative controls for overexpression (OE-NC) and knockdown (sh-NC) were purchased from GeneChem (Shanghai, China). siRNA (50 nM) was transfected using Lipofectamine 3000 (Invitrogen, Carlsbad, CA, USA), according to the manufacturer's instructions. One day before cell transfection, cells were seeded in a 60 mm dish at 3.0×10^5 cells/dish and cultured for 24 h, after which 3 μg plasmid, Lipofectamine 2000 (11668019, Invitrogen, California, USA), and Opti-MEM I (31985062, Gibco, New York, USA) Reduced-Serum Medium were added for cell culture. Next, 8 ng/mL polybrene (TR-1003, Sigma-Aldrich, St. Louis, MO, USA) was added, and cells were cultured for 48 h.

2.8. Chromatin immunoprecipitation (ChIP)

The ChIP procedure includes cell preparation and fixation, ultrasonic chromatin fragmentation, protein and DNA complex immunoprecipitation, elution, crosslinking reversal, and DNA purification and identification. A ChIP kit (Millipore, Billerica, MA, USA) was used according to the manufacturer's instructions to verify the interaction of TAF1 with the APRT promoter. DNA and protein crosslinking was verified using formaldehyde, which was also used for fixation. The DNA segments extracted from ES-2 cells were cut into 200–1000 bp pieces using ultrasound and incubated with TAF1 (1:100, ab10490, Abcam, Cambridge, UK) or IgG antibody. DNA segments were analyzed using Real-time polymerase chain reaction (qRT-PCR).

2.9. RNA-binding protein immunoprecipitation (RIP)

Cells were collected, and nuclei were isolated and precipitated. The chromatin was fragmented, and the RNA-binding protein (RBP)

and bound RNA were used for immunoprecipitation. The unbound material was washed away, and the bound RNA on the immunoprecipitated RBP was purified. The RNA was reverse-transcribed into cDNA and analyzed. The Millipore EZ-Magna RIP RNA kit (Millipore, USA) was used for RIP analysis. ES-2 cells were pre-dissolved in RNase-free RIPA cell lysis buffer (Beyotime). Protein A/G MagBeads were precleaned and incubated with TAF1 antibody (1:100, ab10490, Abcam, Cambridge, UK). Protein A/G MagBeads were incubated overnight with the supernatant, the total RNA was extracted, and the lncRNA FAM225B enrichment was detected by qRT-PCR.

2.10. RNA pull-down

Equilibrium solution (500 μL) was added to the adsorption column by centrifugation. The single target DNA band was cut from the agarose gel, added to an equal volume of solution, and dissolved in a 50 °C water bath for 10 min. The solution was added to the adsorption column for centrifugation, the waste liquid was removed, 600 μL of rinse solution was added to the adsorption column, and the adsorption column was added to the collection tube. The adsorption column CB2 was placed in a new centrifuge tube, 30 μL of elution buffer EB was added to the middle of the adsorption membrane, and the DNA was collected after centrifugation. The Pierce™ Magnetic RNA-Protein Pull-Down Kit (Thermo Fisher, USA) was used according to the manufacturer's instructions. Biotin-labeled lncRNA GAS5, antisense lncRNA GAS5, and RNA for negative control probes were synthesized by GenePharma (www.genepharma.com). The labeled probes that were bound to streptavidin-coated MagBeads were incubated with lysed HK-2 cells. The RNA-protein complex was eluted and separated by SDS-PAGE for the detection of TAF1 expression by western blotting.

2.11. RT-qPCR

Cells in 6 well plates or 100 mg of renal tissue were dissolved in 1 mL Trizol (Thermo Fisher Scientific, MA, USA) and mechanically homogenized. After centrifugation, 200 μL of precooled chloroform was added to the supernatant. After centrifugation, isopropanol was added to the supernatant, followed by centrifugation and ethanol precipitation. Finally, purified water was added to dissolve the pellet of extracted total RNA. M-MLV reverse transcriptase (D7160L; Beyotime, Shanghai, China) and random primers were used for cDNA synthesis. The reaction system was set up according to the Premix Ex *Taq*II kit (Takara, Dalian, China) instructions. RT-PCR was performed using the ABI7500 quantitative PCR system (Applied Biosystems, Shanghai, China), with actin as an internal control for lncRNA and mRNA. Data were analyzed using the $2^{-\Delta\Delta Ct}$ method [21]: $\Delta\Delta Ct = [Ct_{(\text{target gene})}\text{-}Ct_{(\text{internal control})}]_{\text{experimental group}}\text{-}[Ct_{(\text{target gene})}\text{-}Ct_{(\text{internal control})}]_{\text{control group}}$. The primer sequences are listed in Table 1.

2.12. Western blotting

Cells or tissues were lysed, and the total protein concentration was determined using the BCA detection kit (23227, Thermo Fisher Scientific, USA). The proteins were diluted with 5 × loading buffer, the 12 % separation gel was prepared and electrophoresed for 90 min, and proteins were transferred to the membrane for 2 h. Proteins on the membranes were incubated with PBS blocking buffer containing 5 % (w/v) milk powder for 1 h. Next, membranes were incubated overnight at 4 °C with the following primary antibodies: TAF1 (1:300, 50702, Invitrogen, New York, USA), APRT (1:500, ab196558, Cambridge, UK), Bax (1:300, ab32503, Cambridge, UK), Bcl-2 (1:300, ab32124 Cambridge, UK), type I collagen (1:300, ab281974, Cambridge, UK), type IV collagen (1:300, PA5-84585, Invitrogen, New York, USA), LC3-II/LC3-I (1:300, ab192890, Cambridge, UK), p62 (1:300, ab280086, Cambridge, UK), Beclin-1 (1:300, ab210498, Cambridge, UK), and GAPDH (1:500, ab9485, Cambridge, UK). After washing away the excess antibodies, the membranes were incubated with a secondary antibody (1:500, ab114610, Abcam, Cambridge, UK) at room temperature for 1 h. Images were captured using a Bio-Rad Imaging System.

2.13. Transcriptome sequencing

The RNA concentration and purity were determined using the Nanodrop2000, the RNA integrity was determined by electrophoresis, and RNA integrity numbers (RIN) were determined using the Agilent2100. Transcriptome sequencing was performed on an Illumina platform to capture the complete mRNA sequence, which typically has an average length of several kilobases. To achieve this,

Table 1
Primer sequences for reverse transcription polymerase chain reaction.

Name of primer	Sequences (5′-3′)
GAS5-F	GCTAAGGACTCATGAGGAAGCT
GAS5-R	TATTTGGCAAATCTTCTGTTCAAG
TAF1-F	TGGGAAGATGATATCATCTGGG
TAF1-R	TCCAATGTAGCTGTAAAACCTTG
APRT-F	ATCGACTACATCGCAGGTCTG
APRT-R	GCCTTCCCATACTCTAGAGAATAG
ACTIN-F	CGTTGACATCCGTAAAGACCTC
ACTIN-R	TAGGAGCCAGGGCAGTAATCT

F: Forward primer; R: Reverse primer.

mRNA was fragmented using a fragmentation buffer under specific conditions, which generated small fragments of approximately 300 bp. One-stranded cDNA was synthesized from the mRNA using nonspecific primers and reverse transcriptase. Subsequently, the one-stranded cDNA was used as a template to generate two strands. The sticky ends of the cDNA were then flattened by adding End Repair Mix, and an A base was added to the 3' end. After adapter ligation, the resulting products underwent initial screening and fragment selection. The sorted products were amplified using PCR to obtain the final library, which underwent sequencing using the Illumina HiSeq Xten/NovaSeq6000 system. Finally, transcriptome sequencing of the corresponding samples was performed using the Illumina system.

2.14. Bioinformatic analysis

Quality control analysis of raw sequencing data was performed using SeqPrep software (https://github.com/jstjohn/SeqPrep). After achieving quality control, high-quality sequencing data were obtained and compared with the genome in the database using TopHat2 (http://ccb.jhu.edu/software/tophat/index.shtml), followed by another round of quality control. Gene expression was quantified using RSEM software (http://deweylab.github.io/RSEM/) [22]. The number of sequences in the genomic region was determined, and differentially expressed genes (DEGs) between different samples were compared to evaluate the magnitude of gene expression differences. The screening threshold for identifying genes with statistically different expression between samples was set as $|\log2FC| \geq 0$ and a P-value <0.05. The functions of these DEGs were further explored using the Gene Ontology (GO) database (http://www.geneontology.org/). GO is a comprehensive database that summarizes the results of gene studies, defines and describes protein functions and genes, and classifies genes. GO enrichment analysis of DEGs was performed using GOATOOLS software [5]. The Kyoto Encyclopedia of Genes and Genomes (KEGG) (http://www.genome.jp/kegg/) is a knowledge base for systematically analyzing gene

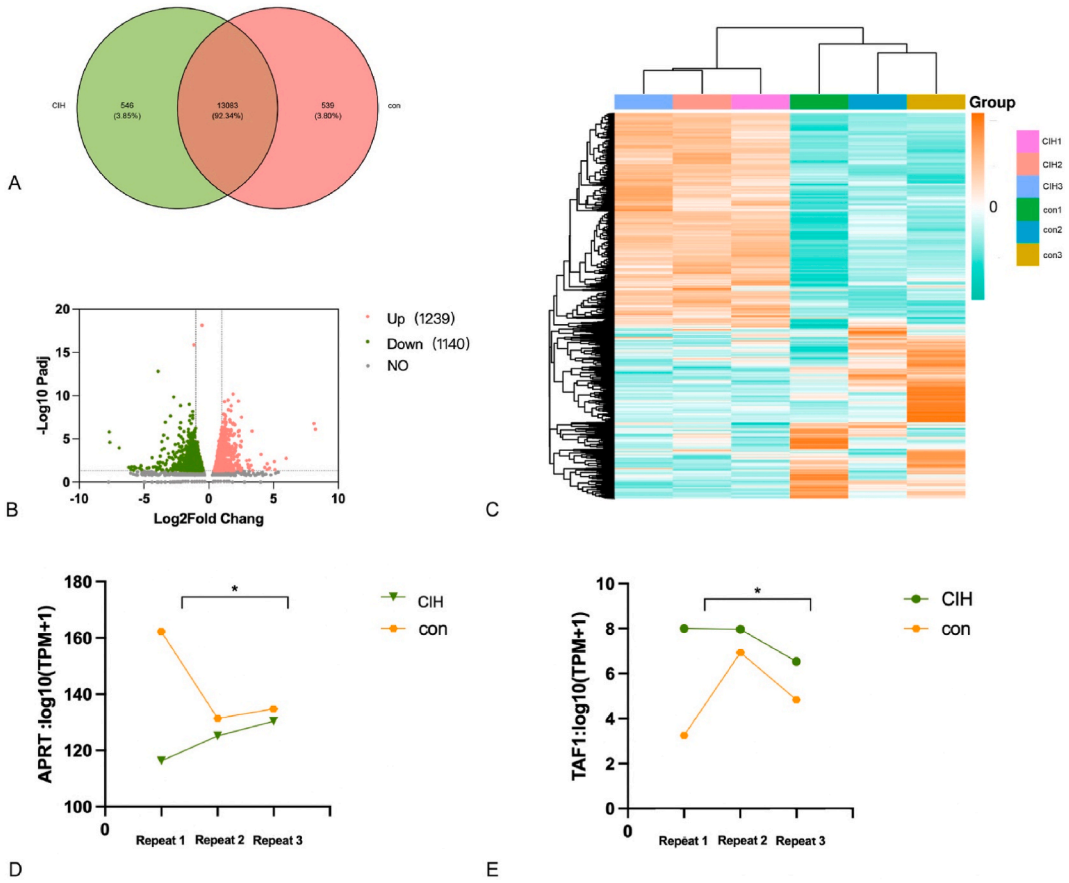

Fig. 1. Analysis of differentially expressed genes. (A) Venn diagram. Green indicates 546 specifically expressed genes in the CIH group, red indicates 539 specifically expressed genes in the control group, and the overlapping green and red indicates 13,083 co-expressed genes. (B) Volcano plot of expression differences. The volcano map is drawn according to the expression of genes, the abscissa is the fold change of gene expression between different groups, and the ordinate is the P-value of differential gene expression between groups. Gray indicates genes with no statistically significant difference, red indicates genes with significantly increased expression, and green indicates genes with significantly decreased expression (the closer to the sides and above). (C) Cluster heatmap. (D): APRT expression was significantly decreased in the CIH group. (E)TAF1 expression was significantly increased in the CIH group. Each row in the graph represents a gene, each column represents a sample, the left side is the gene cluster dendrogram, and below the cluster heatmap is each sample name. *P $<$ 0.05.

function and exploring genomic relevance and functional information. DEGs were further analyzed using KEGG.

2.15. Statistical analysis

Unless otherwise stated, all experiments were performed in triplicate. Data were analyzed using SPSS (version 18.0; IBM Corp., Armonk, New York, USA) and GraphPad Prism (version 8.0; GraphPad Software Inc.). Measurement data are expressed as mean ± standard deviation. A two-tailed paired Student's t-test was used for comparisons between two groups, and one-way analysis of variance with a Tukey's post hoc test was used for multiple comparisons. Statistical significance was set at P-values <0.05.

3. Results

3.1. Analysis of differentially expressed genes (DEGs)

Venn analysis was used to determine the expression of genes in the different sample groups. The Venn diagram showed the co-

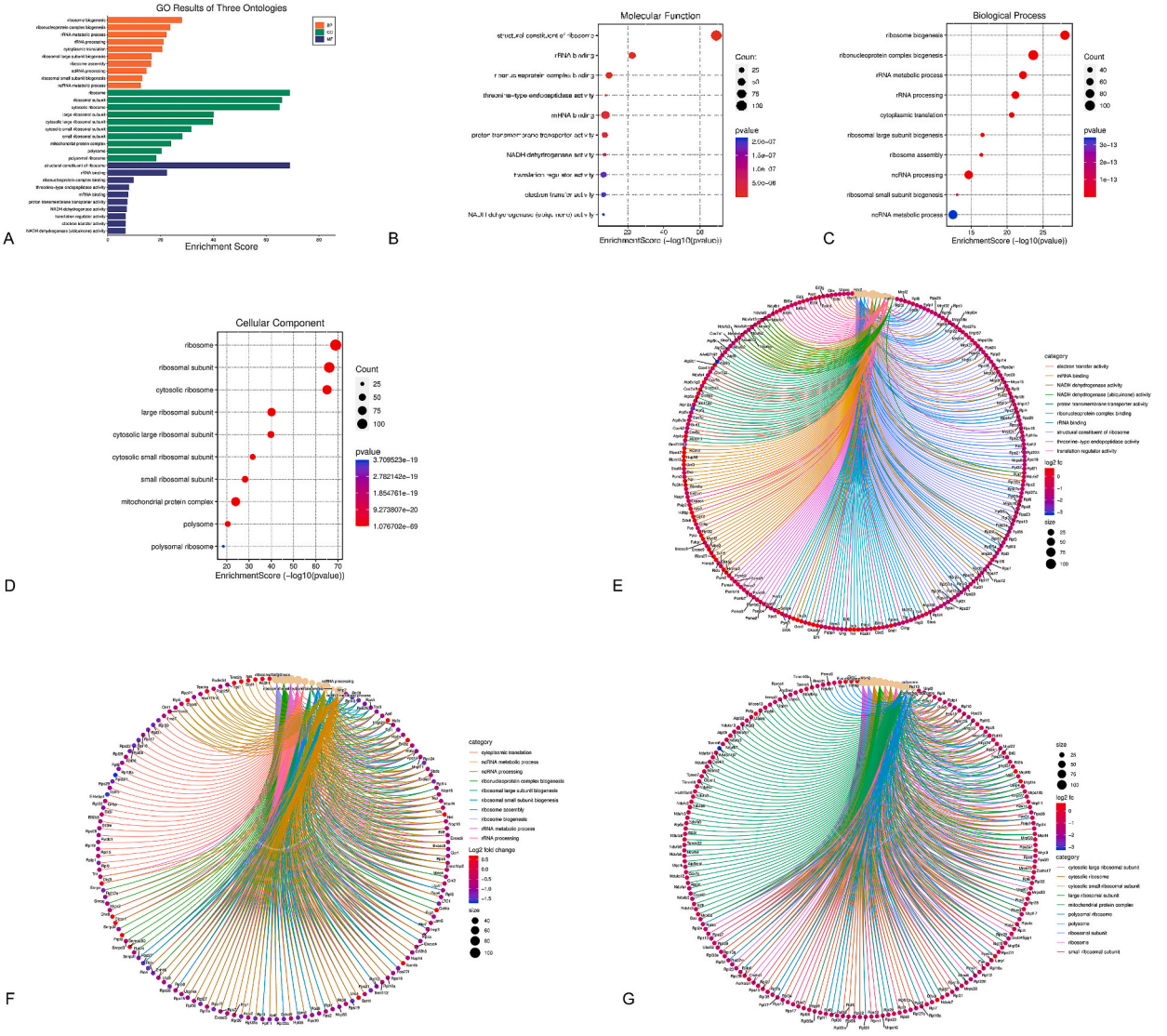

Fig. 2. GO enrichment analysis of differentially expressed genes. (A) GO classification diagram. The abscissa indicates the number of genes with a given function, the ordinate indicates the gene function name, and orange, blue, and green indicate biological process, molecular function, and cell component classifications, respectively. (B) Molecular function enrichment results of differential genes. (C) Biological process enrichment analysis results of differential genes; (D) Cell component enrichment analysis results of differential genes. (E) Molecular function, (F) biological process, (G) cell component enrichment analysis of 2379 DEGs. Genes with P < 0.05 are considered significantly enriched.

expressed and specifically expressed genes in different groups. The analysis found 13,083 co-expressed genes in the SD + CIH and control groups, 546 specifically expressed genes in the CIH group, and 539 specifically expressed genes in the control group (Fig. 1A). Differential expression analysis was used to identify DEGs in different kidney samples. Based on the quantitative expression results, 2379 DEGs were identified in the CIH and control groups, of which 1239 genes were upregulated in the CIH group and 1140 genes were downregulated in the CIH group (Fig. 1B). The cluster heatmap was drawn using the DEG information, and the results indicated that the trend of gene expression in CIH group was close, and the trend of gene expression in control group was close (Fig. 1C). Among them, APRT expression was significantly decreased in the CIH group (Fig. 1D) and TAF1 expression was significantly increased in the CIH group(Fig. 1E).

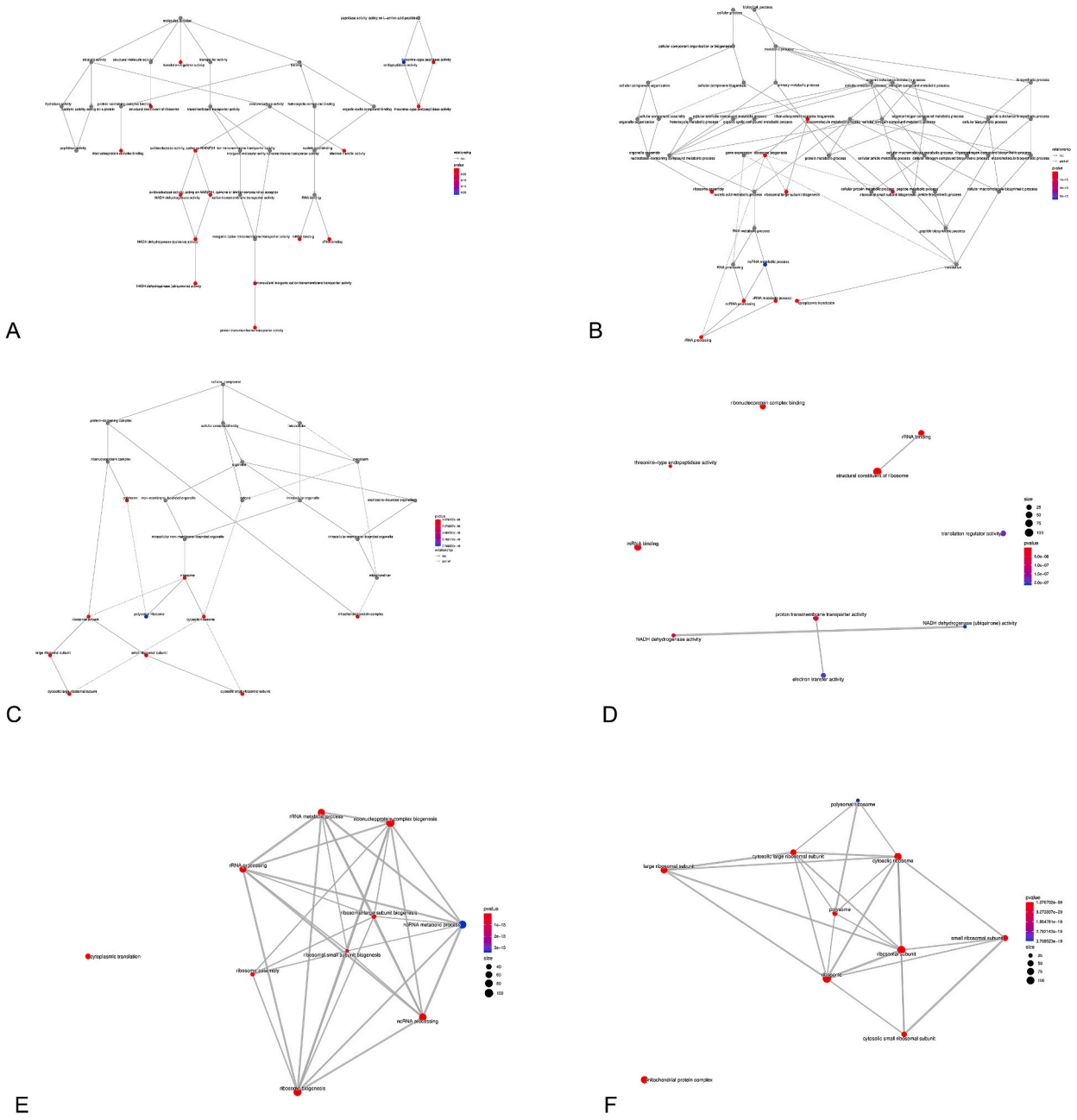

Fig. 3. GOplot and emapplot analyses of differentially expressed genes. GOplot of (A) molecular functions, (B) biological processes, and (C) cell components. emapplot of (D) molecular functions, (E) biological processes, and (F) cell components.

3.2. GO enrichment analysis of DEGs

GO enrichment analysis of DEGs between the CIH and control groups (Fig. 2A) classified and analyzed the functions of DEGs and recorded the function names that were repeated. GO enrichment analysis was divided into cell components, molecular functions, and biological processes, including the top ten secondary classifications. According to GO enrichment analysis, rRNA binding ranked second in molecular function (Fig. 2B); rRNA metabolic process and rRNA processing ranked second and third in biological processes (Fig. 2C), respectively; and ribosomes ranked first in cell components (Fig. 2D), indicating that RNA is significantly involved in the biological process of CIH-mediated kidney injury. The intersection analysis of the Venn plot showed 1239 upregulated genes and 1140 downregulated genes shared by CIH. These 2379 DEGs were possible determining factors for the status of function. GO enrichment analysis indicated that the DEGs mapped to molecular function-related GO terms, such as mRNA-binding and rRNA-binding (Fig. 2E); biological process-related GO terms, such as ncRNA metabolic process and ncRNA processing (Fig. 2F); and cell component-related GO terms, such as cytosolic large ribosomal subunits and ribosomes (Fig. 2G).

3.3. GOplot and emapplot analyses of DEGs

Functional enrichment mapping of the GO enrichment results was performed using GOplot. GOplot suggested that RNA binding is

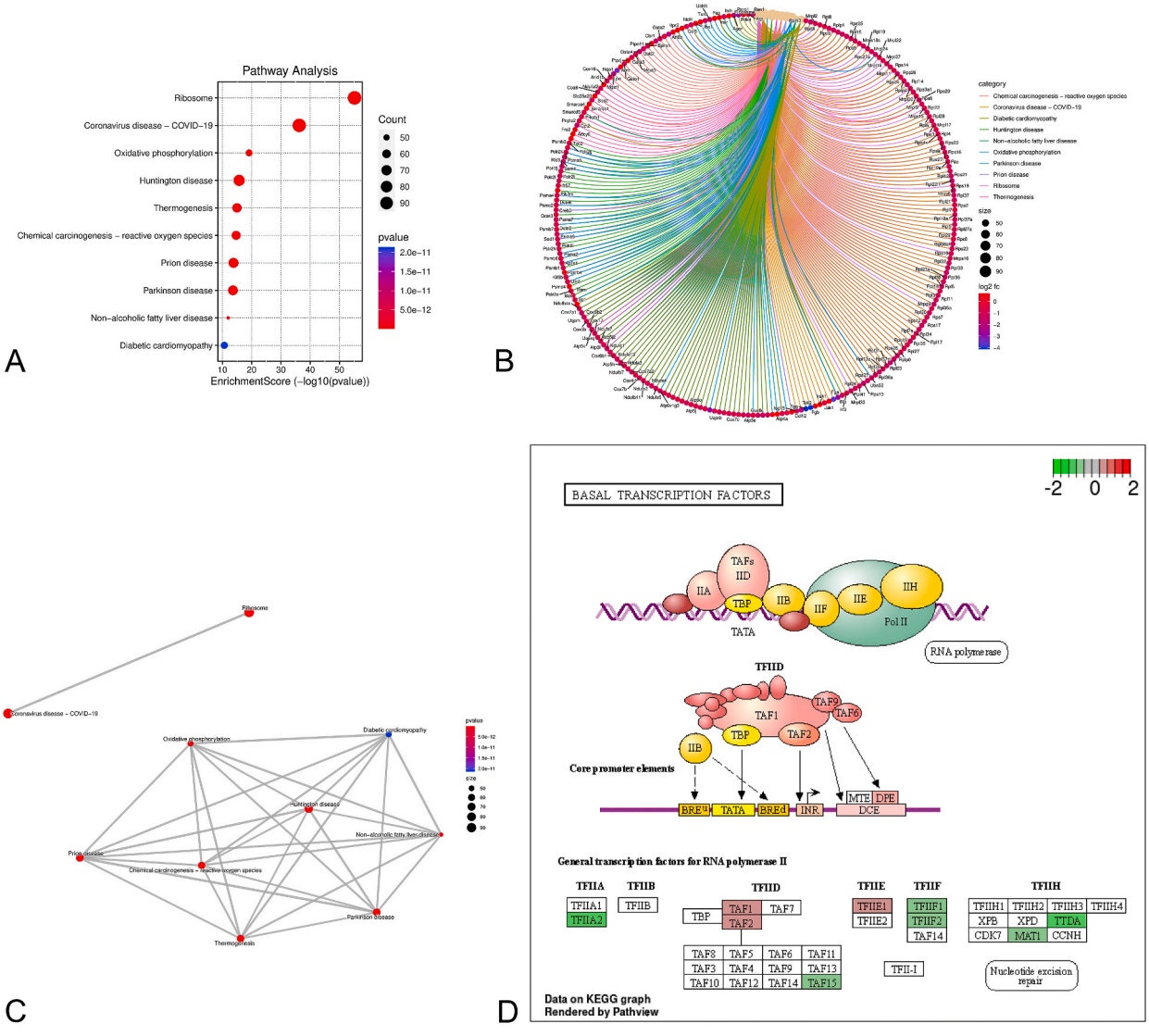

Fig. 4. KEGG enrichment analysis of differentially expressed genes. (A) Plot of KEGG enrichment analysis of differentially expressed genes (DEGs); (B) KEGG enrichment analysis of DEGs, where pathway signals with P-values <0.05 were considered to be significantly enriched; (C) emapplot of KEGG; (D) *TAP1* function and signaling pathway (by bioinformatics).

one of the main molecular functions of DEGs (molecular function GOplot; Fig. 3A), all biological processes were focused on ncRNA metabolic processes and ncRNA processing (biological process GOplot; Fig. 3B), and the cytosol is the main mediator (cell component GOplot; Fig. 3C). The emapplot enrichment map organizes enriched terms into a network that connects overlapping gene sets, which tend to cluster together, allowing the identification of functional modules. The GO enrichment results underwent emapplot mapping. The molecular function emapplot suggested that the main gene set had ribonucleoprotein complex binding, rRNA binding, threonine-type endopeptidase activity, structural constituent of ribosome, translation regulator activity, mRNA binding, proton transmembrane transporter activity, NADH dehydrogenase activity, NADH dehydrogenase activity, and electron transfer activity (Fig. 3D). Biological process emapplott suggested that the main gene functions were more involved than the RNA, including ncRNA metabolic processes, ncRNA processing, rRNA metabolic processes, and rRNA processing (Fig. 3E). The cell component emapplot suggested that the main gene functions were more involved than the polysome (Fig. 3F).

3.4. KEGG enrichment analysis of DEGs

KEGG enrichment analysis of the DEGs in the CIH and control groups revealed that the ribosomal pathway was the most enriched (Fig. 4A). These DEGs were possible determining factors for the status of KEGG signaling pathways. KEGG enrichment results indicated that the DEGs mapped to reactive oxygen species, while CIH was a ROS activator (Fig. 4B). The emapplot mapping of the KEGG enrichment results suggested that more major pathways were involved than ROS (Fig. 4C). KEGG enrichment results suggested that the target gene, *TAF1*, was a basal transcription factor. TAF1, an important subunit of TFIID, recognizes the double acetylated lysine tail of histone H4 through its tandem bromodomain domain and binds to its core promoter sequence to initiate transcription (Fig. 4D).

3.5. GAS5 inhibition or APRT overexpression attenuates CIH-induced renal dysfunction and morphological injury

The interaction between these two factors in CIH-induced renal injury remains unknown. GAS5 and APRT-associated plasmids were injected into rats, and the measurements showed that compared with the sham group, the expression of GAS5 in the kidney tissues of the sh-GAS5 group was suppressed, while the APRT expression in the OE-APRT group was elevated (Fig. 5A and B), indicating successful cell transfection.

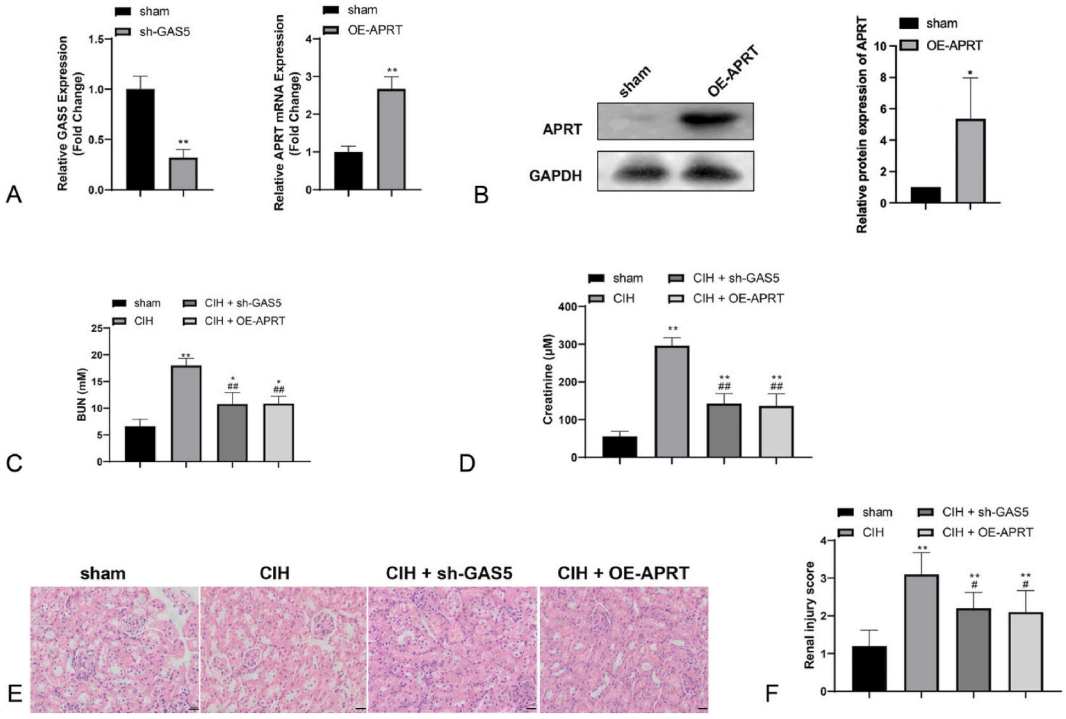

Fig. 5. GAS5 inhibition or APRT overexpression attenuates CIH-induced renal injury. Rats were induced for CIH modeling, and the renal function and morphology were assessed. RT-qPCR (A) and western blotting (B) detected the expression levels of GAS5 and APRT in kidney tissues, indicating successful cell transfection. Full, non-adjusted images proved in the supplementary material. The sh-GAS5 and OE-APRT groups had substantially decreased serum levels of BUN (C) and creatinine (D). H&E staining revealed morphological changes in CIH-induced rats (E). The renal injury was scored on the Jablonski scale (F). (N = 6) *, compared with sham group, $P < 0.05$; **, compared with sham group, $P < 0.01$; #, compared with CIH group, $P < 0.05$; ##, compared with CIH group, $P < 0.01$. CIH, chronic intermittent hypoxia; GAS5: growth arrest-specific transcript 5; APRT: recombinant adenine phosphoribosyl transferase.

The CIH model was established following rat induction, and renal function was assessed by measuring the serum expression levels of BUN and creatinine. The results showed that, compared with rats in the sham group, rats in the CIH group had elevated serum levels of BUN and creatinine, while rats in the sh-GAS5 or OE-APRT groups had substantially decreased levels of BUN and creatinine (Fig. 5C and D). Renal injury was also assessed using H&E staining and a 0–5 Jablonski scale (Fig. 5F). Morphological observations showed that rats in the sham group had normally structured glomeruli and tubules, whereas in the CIH group, the glomeruli were atrophied or necrotic, and the tubules had a thickened basilar membrane with inflammatory cell infiltration (Fig. 5E). H&E staining in the sh-GAS5 and OE-APRT groups showed that the morphology of the glomeruli and tubules was attenuated compared to that in the CIH group (Fig. 5E). These results demonstrated that GAS5 inhibition or APRT overexpression in rats can protect against renal dysfunction and attenuate CIH-induced renal injury.

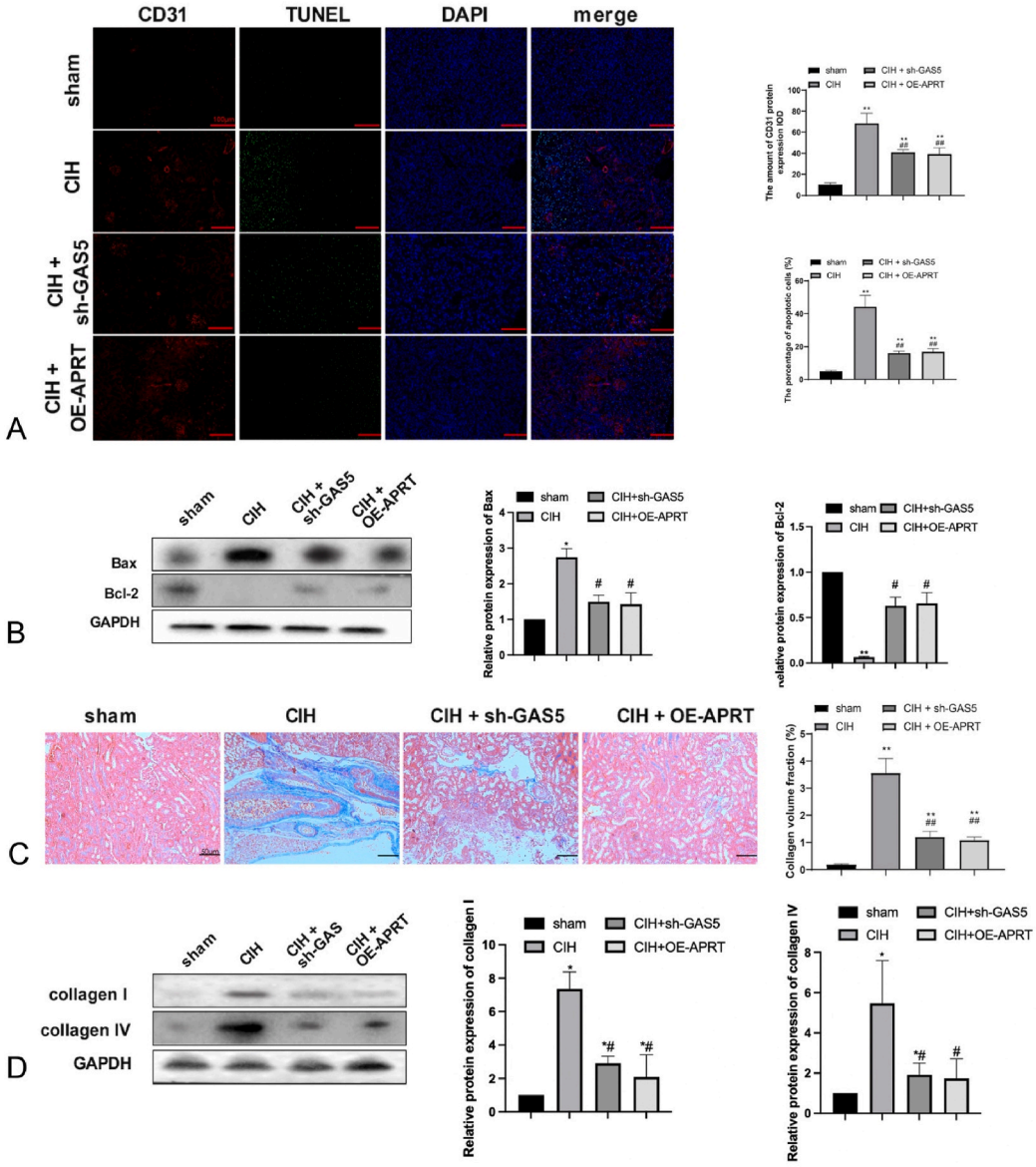

Fig. 6. Attenuation of GAS5 suppression or APRT overexpression in CIH-induced renal tubule cell apoptosis and fibrosis. TUNEL staining to detect apoptosis of renal tubular epithelial cells (red, CD31-positive cells; green, TUNEL-positive cells) shows an increased apoptosis rate in the CIH group (A). The expression levels of apoptosis-related proteins (Bcl-2 and Bax) are detected by western blotting.Full, non-adjusted images proved in the supplementary material. (B). Renal fibrosis is assessed by Masson's staining (C). The expressions of renal fibrosis-related proteins (collagen I and IV) are detected by western blotting. full, non-adjusted images proved in the supplementary material. (D). The collagen expression in kidney tissues is enhanced in the CIH group (N = 6). *, compared with sham group, $P < 0.05$; **, compared with sham group, $P < 0.01$; #, compared with CIH group, $P < 0.05$; ##, compared with CIH group, $P < 0.01$. CIH, chronic intermittent hypoxia; GAS5: growth arrest-specific transcript 5; APRT: recombinant adenine phosphoribosyl transferase.

3.6. GAS5 inhibition or APRT overexpression can ameliorate CIH-induced renal tubular epithelial apoptosis and fibrosis

The effects of GAS5 and APRT on CIH-induced apoptosis were determined using TUNEL staining. The apoptosis rate in rats in the CIH group was higher than that in the sham group, whereas fewer apoptotic cells were found in the sh-GAS5 and OE-APRT groups than in the CIH group (Fig. 6A). Western blot analysis of apoptosis-related proteins demonstrated that rats in the CIH group had decreased Bcl-2 expression and elevated Bax expression compared to the sham group. Meanwhile, compared to the CIH group, Bcl-2 was elevated and Bax was suppressed in the sh-GAS5 and OE-APRT groups (Fig. 6B).

Renal fibrosis in each group was assessed by Masson's staining and western blotting. Masson's staining showed that the collagen expression in kidney tissues was enhanced in the CIH group (vs. sham group) but attenuated in the sh-GAS5 and OE-APRT groups (vs. CIH group) (Fig. 6C). Western blot analysis showed elevated expression of collagen I and IV in the CIH group (vs. sham group), but the expression of collagen I and IV in the sh-GAS5 and OE-APRT groups was lower than that in the CIH group (Fig. 6D). Taken together, the inhibition of GAS5 or overexpression of APRT can attenuate CIH-induced cell apoptosis and renal fibrosis.

3.7. GAS5 inhibition or APRT overexpression suppresses CIH-induced oxidative stress and promotes cell autophagy

To determine how CIH induces apoptosis, we measured the expression of oxidative stress-related factors in renal tissues, including MDA, SOD, GSH-px, and the GSH/GSSG ratio. The measurements showed that the CIH group had elevated MDA expression and decreased SOD and GSH-px activities, as well as a reduced GSH/GSSG ratio, when compared with those of the sham group. Different expression patterns were found in the sh-GAS5 and OE-APRT groups when compared with those in the CIH group (Fig. 7A).

In the event of cell injury, autophagy may be triggered to protect cells. Therefore, we also measured alterations in cell autophagy. Western blot analysis of autophagy-related proteins showed that the CIH group had an elevated LC3-II/LC3-I ratio and p62 expression and no significant change in Beclin-1 expression when compared with those of the sham group. Compared with the CIH group, the sh-GAS5 and OE-APRT groups had substantially elevated LC3-II/LC3-I ratios and Beclin-1 expression, as well as decreased p62 expression (Fig. 7B). These results show that inhibition of GAS5 or APRT overexpression can attenuate CIH-induced cell injury by suppressing oxidative stress and increasing cell autophagy.

3.8. GAS5 binds TAF1 to suppress APRT expression

The expression levels of GAS5 and APRT in the renal tissue were detected. Compared with the sham group, the sh-GAS5 group had elevated APRT expression (Fig. 8A and B), but the GAS5 expression between the sham and OE-APRT groups showed no significant difference ($P > 0.05$). Therefore, we speculated that GAS5 may be located upstream of APRT and regulate APRT expression.

We further measured the expression of TAF1 in renal tissues and found that compared to the sham group, the expression of TAF1 in renal tissue in the CIH group was substantially elevated (Fig. 8C and D).

The RNA pull-down assay was used to collect proteins that can bind GAS5 in HK-2 cells, and the expression of TAF1 was detected by western blotting. The results showed that TAF1 binds to GAS5 (Fig. 8E). RIP analysis showed that GAS5 directly interacted with TAF1 in ES-2 cells (Fig. 8F). ChIP revealed an enriched APRT promoter in the complex pulled down by the TAF1 antibody (Fig. 8G),

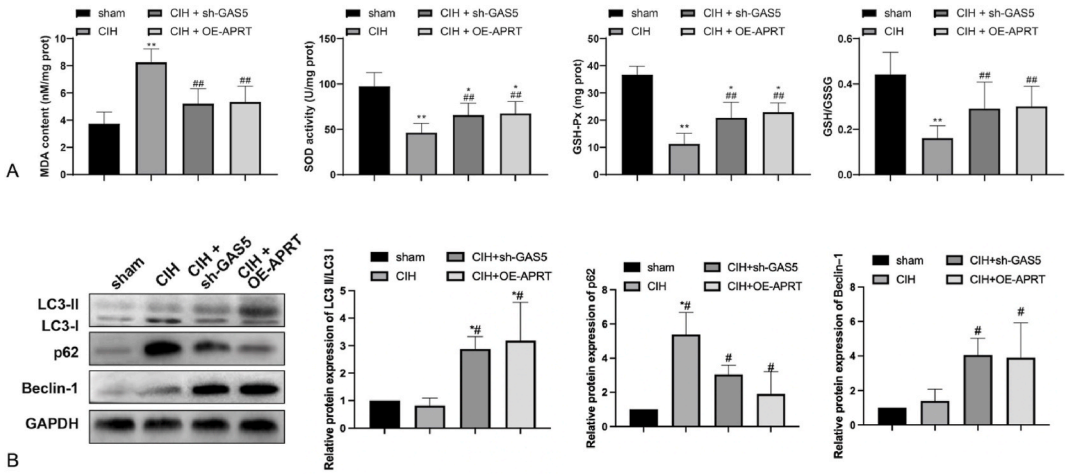

Fig. 7. CIH-induced oxidative stress is decreased and autophagy is increased by GAS5 inhibition or APRT overexpression. The expressions of oxidative stress-related factors in renal tissues, including MDA, SOD, GSH-px, and the GSH/GSSG ratio were determined by a detection kit, and the oxidative stress was increased in the CIH group (A); The expression levels of cell autophagy-related proteins, LC3-II/LC3-I ratio, p62, and Beclin-1, are detected by western blotting. Autophagy is increased in the CIH group. Full, non-adjusted images proved in the supplementary material (B). ($N = 6$) *$P < 0.05$, **$P < 0.01$. CIH, chronic intermittent hypoxia; GAS5: growth arrest-specific transcript 5; APRT: recombinant adenine phosphoribosyl transferase.

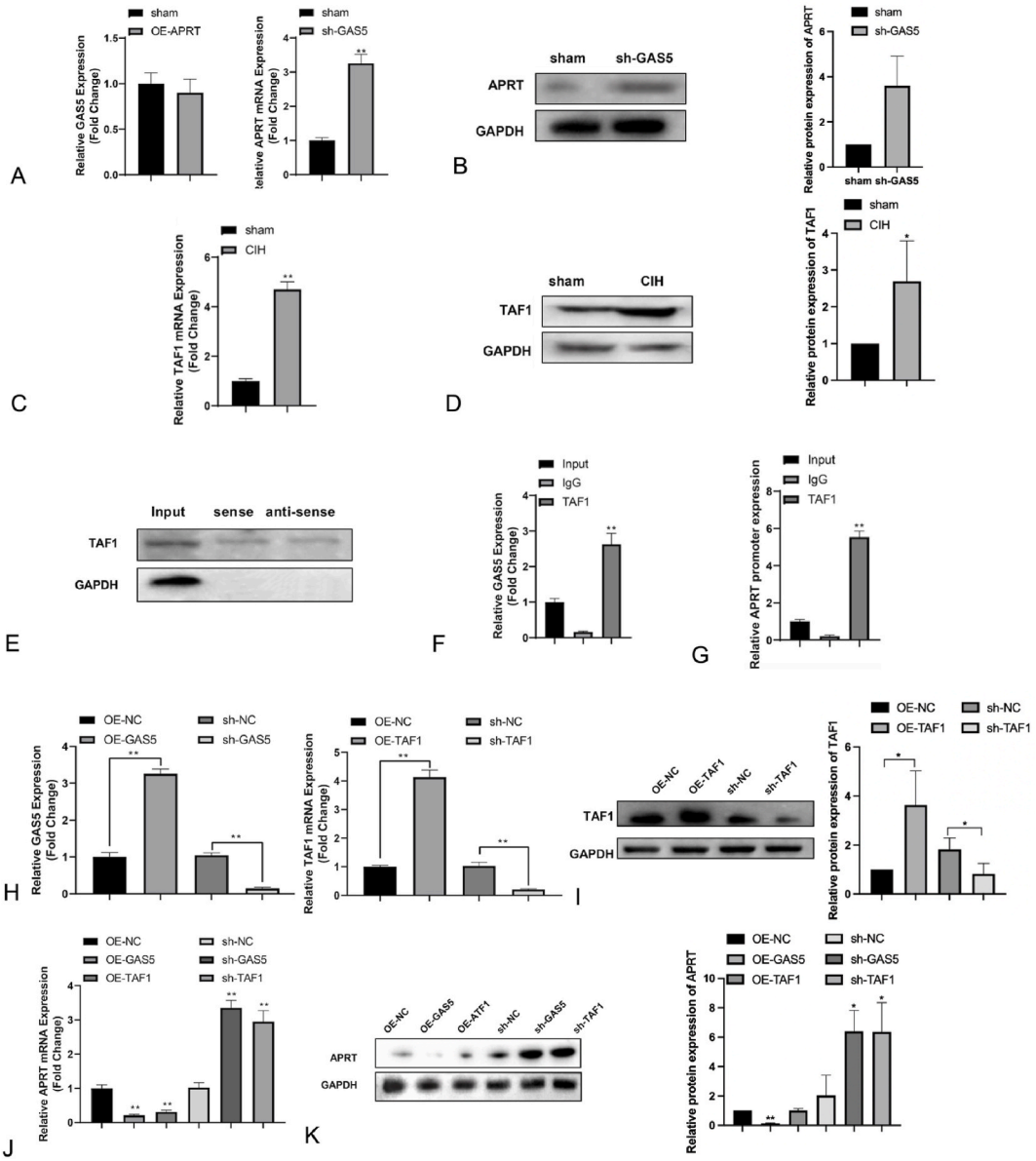

Fig. 8. GAS5 binds TAF1 to suppress APRT transcription. RT-qPCR (A) and western blotting (B) are used to detect the expression of GAS5 and APRT in renal tissues. RT-qPCR (C) and western blotting (D) detect the expression of TAF1 in renal tissues. RNA pull-down (E) and RIP (F) detect the binding of GAS5 and TAF1. ChIP verifies the binding of TAF1 with the APRT promoter (G). After cell transfection, RT-qPCR (H) and western blotting (I) detect the transfection efficiency. RT-qPCR (J) and western blotting (K) detect the APRT expression level. (N = 3) *P < 0.05, **P < 0.01. CIH, chronic intermittent hypoxia; GAS5: growth arrest-specific transcript 5; APRT: recombinant adenine phosphoribosyl transferase; TAF1: TATA-box binding protein associated factor 1.

indicating that TAF1 is an APRT promoter.

To verify the role of GAS5 and TAF1 in APRT expression, we measured APRT expression after cell transfection in HK-2 cells (Fig. 8H and I). RT-qPCR and western blotting showed that compared with the OE-NC group, the OE-GAS5 and OE-TAF1 groups had decreased APRT expression, while compared with the sh-NC group, APRT expression in the sh-GAS5 and sh-TAF1 groups was elevated (Fig. 8J and K). Taken together, lncRNA GAS5 may bind to TAF1 to suppress APRT expression, thus promoting CIH-induced renal injury.

4. Discussion

OSAHS is detrimental to renal function [23], and renal hypoxia, endothelial dysfunction, and increased oxidative stress have been proposed as possible mechanisms underlying OSAHS-associated renal dysfunction. In our study, sequencing analysis suggested that

RNA is deeply involved in the biological process of CIH-mediated kidney injury, TAF1 is significantly increased in the CIH group, APRT is significantly reduced in the CIH group, and inhibition of GAS5 expression or APRT overexpression can attenuate CIH-induced renal injury. Further mechanistic experiments demonstrated that GAS5 binds to TAF1 to negatively regulate APRT expression.

Similar to the uncontrolled proliferation of tumor cells, renal fibrosis is characterized by unchecked proliferation of interstitial fibroblasts and excessive extracellular matrix (ECM) events [24]. Furthermore, GAS5 is down-regulated in TGF-β-treated renal tubular epithelial cells and mediates miR-21/MMP2/9 to attenuate kidney fibrosis [24]. In contrast, GAS5 exacerbates renal tubular epithelial fibrosis by binding to miR-96-5p [25]. In addition, different GAS5 expression patterns have been found in mouse models of diabetic nephropathy and unilateral ureteric obstruction models [26], which can be explained by the different mechanisms of renal injury. In our study, we knocked down GAS5 expression in CIH-induced rat models, in which the renal function and renal tissue morphology were attenuated, and the apoptosis, fibrosis, oxidative stress, and autophagy of renal tubular epithelial cells were measured. Taken together, these results demonstrate that inhibiting GAS5 expression can attenuate CIH-induced renal injury. The protective effect of GAS5 silencing against hypoxia-induced apoptosis and cell viability has been verified in both cardiomyocytes [27] and hippocampal neurons [28]. However, high-glucose induced HK-2 cells show inconsistent results, which demonstrates that GAS5 overexpression can suppress reactive oxygen species, inflammation, and pyroptosis. lncRNAs improve diabetic nephropathy by changing the miRNA expression [29], while consistent results in HK-2 cells have also found that GAS5 knockout attenuates cellular toxicity and apoptosis [30]. A study constructed a ceRNA network associated with renal fibrosis and found a target gene of lncRNA GAS5 that may regulate renal fibrosis, providing experimental evidence supporting the use of GAS5 targeting to treat renal fibrosis [31]. Another study revealed an association between the rs145204276 polymorphism in the lncRNA GAS5 and the risk of developing renal cell carcinoma; therefore, GAS5 is a potentially viable biomarker for identifying individuals at risk of developing this form of renal cell carcinoma [32]. These controversial results prompted us to explore possible downstream targets of GAS5 in CIH-induced renal injury.

APRT deficiency is a hereditary purine metabolism disorder that causes CKD, and timely diagnosis and treatment of APRT deficiency can decrease renal complications and preserve kidney function [16]. Our study also showed that APRT overexpression can attenuate CIH-induced renal injury. In this study, APRT overexpression mitigated fibrosis, autophagy, oxidative stress, and apoptosis in renal tubular epithelial cells. Recently, a case report of renal calculus disease reported APRT deficiency in patients with crystal nephropathy and end-stage renal failure [33]. In our study, we also measured the expression of APRT in cells transfected with sh-GAS5 and showed that suppression of GAS5 elevates APRT expression, whereas APRT overexpression has no effect on GAS5 expression. In addition, LncMAP analysis revealed that GAS5 in papillary renal cell carcinoma can bind to the transcription factor TAF1 to suppress APRT transcription. Therefore, we investigated the possible mechanism of action of GAS5/APRT in CIH-induced renal injury. TAF1 mediates protein phosphorylation, histone acetylation, and recognition of the acetylated histone tail [34]. Transcription factors (TFs) are a group of proteins responsible for multiple cellular processes, and their deregulation is associated with disease progression [35]. TAF1 is a co-activator of androgen receptors that is associated with prostate cancer progression [36]. In this study, KEGG enrichment analysis of DEGs suggested that TAF1 is a basal TF. TAF1, as an important subunit of TFIID, recognizes double-acetylated histone H4 through its tandem bromodomain domain and binds to the core promoter sequence to initiate transcription. To our knowledge, this is the first study to identify the role of TAF1 in CIH-induced renal injury. Further experiments showed that GAS5 can bind to TAF1 to negatively mediate APRT expression. In summary, lncRNA GAS5 inhibits APRT transcription by binding TAF1 to promote the renal injury caused by chronic intermittent hypoxia, and GAS5 and APRT are potential therapeutic targets for renal injury. This research did not involve clinical studies and therefore had some confounding factors. However, some details should be noted, such as maintaining the standardization of each operation step to reduce errors and the occurrence of confounding factors.

5. Conclusion

This study revealed the role of GAS5 and APRT in CIH-induced renal injury. In vivo, inhibition of GAS5 expression and elevation of APRT expression can alleviate renal injury in rats, such as atrophy or necrosis of the glomerulus and thickening of the tubular basilar membrane with inflammatory cell infiltration. In vitro inhibition of GAS5 expression elevates APRT expression and attenuates CIH-induced cell fibrosis, autophagy, and oxidative stress in renal tubular epithelial cells by binding to TAF1. GAS5 and APRT are potential therapeutic targets for renal injury; however, more evidence and data are required before the function of GAS5 in the regulation of renal injury is fully understood.

Funding

This work was supported by the Hubei Provincial Natural Science Foundation of China (2024AFB050) , the National Key R&D Program of China (2021YFC2500702) and the National Natural Science Foundation of China (82270104,82201268). Health Commission of Hubei Province Scientific Research Project (WJ2023Z010); Young Doctors' Innovation and Development Program (HXQNJJ-2023-010); Moderate and Severe Asthma Diagnosis and Treatment of Scientific Research Project (Z001).

Data sharing statement

Data included in article.

Consent for publication

Not applicable.

CRediT authorship contribution statement

Wei Liu: Writing – review & editing, Writing – original draft. **Wukaiyang Liang:** Formal analysis. **CunTai Zhang:** Software. **Huiguo Liu:** Formal analysis. **Hai Li:** Methodology. **Lun Zhou:** Writing – review & editing. **Ling Zhou:** Writing – review & editing, Conceptualization.

Declaration of competing interest

The authors declare that they have no known competing financial interests or personal relationships that could have appeared to influence the work reported in this paper.

Acknowledgements

WL wrote the main manuscript text, W L and LL reviewed the experimental data and edited the manuscript for important intellectual inputs; CZ reiewed the experimental data. HL assist this study, interpreted the experimental findings, SW and LZ edited the manuscript for important intellectual contents. All authors were involved in experimental de-sign, data interpretation, and manuscript preparation. All authors read and approved the final manuscript. *Figdraw* was used for figures.

Abbreviations

OSAHS	obstructive sleep apnea hypopnea syndrome
CIH	chronic intermittent hypoxia
GAS5	growth arrest-specific transcript 5
APRT	recombinant adenine phosphoribosyl transferase
TAF1	TATA-box binding protein associated factor 1
BUN	blood urea nitrogen
CKD	chronic kidney diseases
RAAS	renin-angiotensin-aldosterone system
TFIID	transcription factor IID
SOD	super oxidedismutase
MDA	malondialdehyde
GSH-Px	glutathione Peroxidase
GSSG	glutathione disulfide
OE	overexpression
ChIP	chromatin Immunoprecipitation
RIP	RNA Binding Protein Immunoprecipitation

Appendix A. Supplementary data

Supplementary data to this article can be found online at https://doi.org/10.1016/j.heliyon.2024.e33084.

References

[1] D.J. Gottlieb, Screening for obstructive sleep apnea in adults, JAMA 328 (19) (2022) 1908–1910.
[2] W. Liu, L. Zhou, D. Zhao, X. Wu, F. Yue, H. Yang, M. Jin, M. Xiong, K. Hu, Development and validation of a prognostic nomogram in lung cancer with obstructive sleep apnea syndrome, Front. Med. 9 (2022) 810907.
[3] C.H. Lin, R.C. Lurie, O.D. Lyons, Sleep apnea and chronic kidney disease: a state-of-the-art review, Chest 157 (3) (2020) 673–685.
[4] W. Liu, D. Zhao, X. Wu, F. Yue, H. Yang, K. Hu, Rapamycin ameliorates chronic intermittent hypoxia and sleep deprivation-induced renal damage via the mammalian target of rapamycin (mTOR)/NOD-like receptor protein 3 (NLRP3) signaling pathway, Bioengineered 13 (3) (2022) 5537–5550.
[5] P. Pochetti, D. Azzolina, B. Ragnoli, P.A. Tillio, V. Cantaluppi, M. Malerba, Interrelationship among obstructive sleep apnea, renal function and survival: a cohort study, Int. J. Environ. Res. Publ. Health 17 (14) (2020).
[6] C.P.C. Ow, J.P. Ngo, M.M. Ullah, L.M. Hilliard, R.G. Evans, Renal hypoxia in kidney disease: cause or consequence? Acta Physiol. 222 (4) (2018) e12999.
[7] D. Sun, Z. Yu, X. Fang, M. Liu, Y. Pu, Q. Shao, D. Wang, X. Zhao, A. Huang, Z. Xiang, C. Zhao, R.J. Franklin, L. Cao, C. He, LncRNA GAS5 inhibits microglial M2 polarization and exacerbates demyelination, EMBO Rep. 18 (10) (2017) 1801–1816.
[8] Y. Zhou, B. Chen, GAS5-mediated regulation of cell signaling, Mol. Med. Rep. 22 (4) (2020) 3049–3056 (Review).
[9] X. Dong, W. Gao, X. Lv, Y. Wang, Q. Wu, Z. Yang, G. Mao, W. Xing, Association between lncRNA GAS5, MEG3, and PCAT-1 polymorphisms and cancer risk: a meta-analysis, Dis. Markers 2020 (2020) 6723487.

[10] K. Cheng, Z. Zhao, G. Wang, J. Wang, W. Zhu, lncRNA GAS5 inhibits colorectal cancer cell proliferation via the miR-182-5p/FOXO3a axis, Oncol. Rep. 40 (4) (2018) 2371–2380.
[11] X. Dong, C. Kong, X. Liu, J. Bi, Z. Li, Z. Li, Y. Zhu, Z. Zhang, GAS5 functions as a ceRNA to regulate hZIP1 expression by sponging miR-223 in clear cell renal cell carcinoma, Am. J. Cancer Res. 8 (8) (2018) 1414–1426.
[12] H.P. Qiao, W.S. Gao, J.X. Huo, Z.S. Yang, Long non-coding RNA GAS5 functions as a tumor suppressor in renal cell carcinoma, Asian Pac. J. Cancer Prev. APJCP 14 (2) (2013) 1077–1082.
[13] W. Yang, K. Zhang, L. Li, K. Ma, B. Hong, Y. Gong, K. Gong, Discovery and validation of the prognostic value of the lncRNAs encoding snoRNAs in patients with clear cell renal cell carcinoma, Aging (Albany NY) 12 (5) (2020) 4424–4444.
[14] Y. Guo, G. Li, L. Gao, X. Cheng, L. Wang, Y. Qin, D. Zhang, Exaggerated renal fibrosis in lncRNA Gas5-deficient mice after unilateral ureteric obstruction, Life Sci. 264 (2021) 118656.
[15] J. Yesodharan, N.V. Seethalekshmy, R.R. Nair, Recurrent DHA nephropathy in renal allograft-revisiting clinicopathological aspects of a rare entity, Indian J. Pathol. Microbiol. 64 (3) (2021) 504–508.
[16] H.L. Runolfsdottir, R. Palsson, I.M. Agustsdottir, O.S. Indridason, V.O. Edvardsson, Long-term renal outcomes of APRT deficiency presenting in childhood, Pediatr. Nephrol. 34 (3) (2019) 435–442.
[17] S. Bhattacharya, X. Lou, P. Hwang, K.R. Rajashankar, X. Wang, J.A. Gustafsson, R.J. Fletterick, R.H. Jacobson, P. Webb, Structural and functional insight into TAF1-TAF7, a subcomplex of transcription factor II D, Proc. Natl. Acad. Sci. U. S. A. 111 (25) (2014) 9103–9108.
[18] Y. Song, H. Zhang, Z. Song, Y. Yang, S. Zhang, W. Wang, S. Zhang, Long noncoding RNA GAS5 inhibits osteogenic differentiation through MicroRNA 382-3p/TAF1 signaling, Mol. Cell Biol. 42 (2) (2022) e0054120.
[19] L. Liang, D. Zheng, C. Lu, Q. Xi, H. Bao, W. Li, Y. Gu, Y. Mao, B. Xu, X. Gu, Exosomes derived from miR-301a-3p-overexpressing adipose-derived mesenchymal stem cells reverse hypoxia-induced erectile dysfunction in rat models, Stem Cell Res. Ther. 12 (1) (2021) 87.
[20] C.F. Islam, R.T. Mathie, M.D. Dinneen, E.A. Kiely, A.M. Peters, P.A. Grace, Ischaemia-reperfusion injury in the rat kidney: the effect of preconditioning, Br. J. Urol. 79 (6) (1997) 842–847.
[21] B. Burja, T. Kuret, T. Janko, D. Topalovic, L. Zivkovic, K. Mrak-Poljsak, B. Spremo-Potparevic, P. Zigon, O. Distler, S. Cucnik, S. Sodin-Semrl, K. Lakota, M. Frank-Bertoncelj, Olive leaf extract attenuates inflammatory activation and DNA damage in human arterial endothelial cells, Front Cardiovasc Med 6 (2019) 56.
[22] B. Li, C.N. Dewey, RSEM: accurate transcript quantification from RNA-Seq data with or without a reference genome, BMC Bioinf. 12 (2011) 323.
[23] M. Perticone, R. Maio, P.E. Scarpino, L. Mancuso, M. Volpentesta, B. Caroleo, E. Suraci, A. Sciacqua, G. Sesti, F. Perticone, Continuous positive airway pressure improves renal function in obese patients with obstructive sleep apnea syndrome, Front. Med. 8 (2021) 642086.
[24] Y. Yu, H. Jiang, Y. Niu, J. Huang, X. Zhang, X. Liu, Y. Zhang, S. Liu, H. Fu, C. Yu, Long noncoding RNA-GAS5 retards renal fibrosis through repressing miR-21 activity, Exp. Mol. Pathol. 116 (2020) 104518.
[25] W. Wang, Y.J. Jia, Y.L. Yang, M. Xue, Z.J. Zheng, L. Wang, Y.M. Xue, LncRNA GAS5 exacerbates renal tubular epithelial fibrosis by acting as a competing endogenous RNA of miR-96-5p, Biomed. Pharmacother. 121 (2020) 109411.
[26] L. Zhang, S. Zhao, Y. Zhu, Long noncoding RNA growth arrest-specific transcript 5 alleviates renal fibrosis in diabetic nephropathy by downregulating matrix metalloproteinase 9 through recruitment of enhancer of zeste homolog 2, FASEB J 34 (2) (2020) 2703–2714.
[27] J. Du, S.T. Yang, J. Liu, K.X. Zhang, J.Y. Leng, Silence of LncRNA GAS5 protects cardiomyocytes H9c2 against hypoxic injury via sponging miR-142-5p, Mol Cells 42 (5) (2019) 397–405.
[28] R.B. Zhao, L.H. Zhu, J.P. Shu, L.X. Qiao, Z.K. Xia, GAS5 silencing protects against hypoxia/ischemia-induced neonatal brain injury, Biochem. Biophys. Res. Commun. 497 (1) (2018) 285–291.
[29] C. Xie, W. Wu, A. Tang, N. Luo, Y. Tan, lncRNA GAS5/miR-452-5p reduces oxidative stress and pyroptosis of high-glucose-stimulated renal tubular cells, Diabetes Metab Syndr Obes 12 (2019) 2609–2617.
[30] L. Lv, D. Li, F. Tian, X. Li, Z. Jing, X. Yu, Silence of lncRNA GAS5 alleviates high glucose toxicity to human renal tubular epithelial HK-2 cells through regulation of miR-27a, Artif. Cells, Nanomed. Biotechnol. 47 (1) (2019) 2205–2212.
[31] H. Su, J. Xie, L. Wen, S. Wang, S. Chen, J. Li, C. Qi, Q. Zhang, X. He, L. Zheng, L. Wang, LncRNA Gas5 regulates Fn1 deposition via Creb5 in renal fibrosis, Epigenomics 13 (9) (2021) 699–713.
[32] X. Xiang, L. Chen, J. He, G. Ma, Y. Li, LncRNA GAS5 rs145204276 polymorphism reduces renal cell carcinoma susceptibility in southern Chinese population, J. Inflamm. Res. 15 (2022) 1147–1158.
[33] M. Sharma, S. Gowrishankar, T.K. Jeloka, A rare case of APRT deficiency with end-stage renal failure and successful renal transplant, Indian J. Nephrol. 31 (1) (2021) 57–60.
[34] H. Wang, E.C. Curran, T.R. Hinds, E.H. Wang, N. Zheng, Crystal structure of a TAF1-TAF7 complex in human transcription factor IID reveals a promoter binding module, Cell Res. 24 (12) (2014) 1433–1444.
[35] E. Mondragon, L.J. Maher 3rd, Anti-transcription factor RNA aptamers as potential therapeutics, Nucleic Acid Ther 26 (1) (2016) 29–43.
[36] P. Tavassoli, L.A. Wafa, H. Cheng, A. Zoubeidi, L. Fazli, M. Gleave, R. Snoek, P.S. Rennie, TAF1 differentially enhances androgen receptor transcriptional activity via its N-terminal kinase and ubiquitin-activating and -conjugating domains, Mol. Endocrinol. 24 (4) (2010) 696–708.